JOURNAL OF GEOPHYSICAL RESEARCH, VOL. 87, NO. C12, PAGES 9467–9476, NOVEMBER 20, 1982

# Gulf Stream Meanders: Observations on Propagation and Growth

D. RANDOLPH WATTS AND WILLIAM E. JOHNS

*Graduate School of Oceanography, University of Rhode Island, Kingston, Rhode Island 02881*

We present a new method for continuously tracking the location of the Gulf Stream using a moored array of inverted echo sounders. Time series of lateral displacements of the front, shown accurate to ±8 km, have been collected along three sections spaced 100, 150, and 200 km downstream (NE) of Cape Hatteras, North Carolina, for a period of 12 months. These records are highly coherent at all periodicities longer than 4 days. From the observed phase lags, a dispersion relationship is presented for the meanders: As the period and wavelength ($T$, $\lambda$) increase from (4 days, 180 km) to (30 days, 600 km), the phase speed decreases smoothly from 40 to 20 km $d^{-1}$. The meanders exhibited rapid growth at periods longer than 4 days, doubling in variance in each 50-km step downstream. This downstream growth is most appropriately described by a spatial $e$-folding scale $\kappa^{-1} \sim 400$ km for $(T, \lambda) \lesssim$ (9 days, 300 km), and a temporal $e$-folding scale $\sigma^{-1} \sim 6$ days for $(T, \lambda) \gtrsim$ (14 days, 400 km).

## INTRODUCTION

During 1979–1980 we have collected a 12-month record from an array of seven inverted echo sounders (IES) and three deep current meters deployed 100 to 200 km northeast of Cape Hatteras in 2000–4000 m water. This array continuously monitored the path of the Gulf Stream and the deep currents under it. On four deployment and recovery cruises to the area, expendable bathythermograph traces (XBT) and hydrographic data were collected to survey the temperature and density structure along the stream path and on sections normal to it.

After a brief review of earlier studies on meanders, this paper presents a discussion of the measurement techniques using IES in the Gulf Stream. We show by direct comparisons with traditional measurement methods that (1) each IES produces a continuous record of the thermocline depth (here taken to be the 15°C isotherm for subsequent comparison with standard methods of determining the position of the 'north wall' of the stream) with accuracy of 20 m in a range of variation of 800 m, and (2) the array of IES's paired across the stream produces continuous estimates of the stream position with 8 km accuracy. The results from the three IES sections located 100, 150, and 200 km downstream of Cape Hatteras show very high coherence throughout the array with rapid (20 to 40 km $d^{-1}$) translation of the meanders downstream accompanied by rapid growth of the lateral displacements, doubling in variance with each 50-km step downstream. In a companion paper (W. E. Johns and D. R. Watts, manuscript in preparation, 1982) we discuss the current meter records and the relationship of the deep currents to Gulf Stream meanders.

## HISTORICAL BACKGROUND

The Gulf Stream emerges from the Florida Straits bounded to the west by the continental margin (200-m isobath) and flows northward to the Carolinas in mean depths of 500–800 m. Off Onslow Bay near 34°N, the Blake Plateau ends and the continental slope descends steeply to 2000–4000 m depth. Downstream of Cape Hatteras the stream no longer follows the shelf break. Instead, the mean path continues to the northeast into ever deepening waters. Within 300 km downstream of Cape Hatteras the mean water depth below the stream is greater than 4000 m, and the current is bounded on the northwest by a widening wedge of relatively stationary Slope Water rather than a solid coastal boundary.

The instantaneous path of the stream differs from the above mean description. The motion is characterized by meanders, appearing as lateral shifts of the entire baroclinic structure associated with the Gulf Stream. South of Cape Hatteras, the root mean square lateral displacements increase slowly from 5–10 km off Florida, to a local maximum of 25 km downstream of a topographic feature off Charleston, South Carolina (the 'Charleston Bump,' 31°–32°N), in the lee of which they decay back to 10-km rms [*Bane and Brooks,* 1979]. Meanders along the Carolina shelf have been tracked by satellite [*Legeckis,* 1979] and by XBT and moored current meters [*Brooks and Bane,* 1981; *Bane et al.* 1981]; they have wavelengths of 150–200 km and propagate downstream at rates of approximately 30–40 km $d^{-1}$.

Downstream of Cape Hatteras the envelope of meandering broadens greatly to 200–300 km (Figure 1), and the stream can shift through more than its own width. In the early shipboard surveys [*Fuglister and Worthington,* 1951; *Fuglister,* 1963] the path of the stream south of Nova Scotia was dominated by long-wavelength (~400 km), large-amplitude meanders. Those which were studied in detail were found to be quasi-stationary and were characterized by a slowly evolving baroclinic field, indicating temporal growth. Farther upstream near 72°W, however, significant eastward propagation was observed; one meander crest moved at a rate of approximately 17 km $d^{-1}$ for 3 days [*Fuglister and Worthington,* 1951]. *Hansen* [1970] later conducted monthly path surveys between 75° and 55°W for 1 year, with weekly surveys over a 2-month period, using a towed thermistor. He found meanders on appreciably shorter scales, with wavelengths ranging from 200 to 400 km. Mean downstream propagation rates of 5–10 cm $s^{-1}$ and spatial growth rates of $2 \times 10^{-3}$ $km^{-1}$ were estimated by constructing lines of constant phase between features on successive path sequences. The rapid evolution between monthly paths, however, produced considerable ambiguity in identifying and tracking events. Weekly paths evolved more continuously and were apparently not aliased by higher-frequency/wave number phenomena.

In a subsequent study, *Robinson et al.* [1974] constructed



Paper number 2C1300.
0148-0227/82/002C-1300$05.00

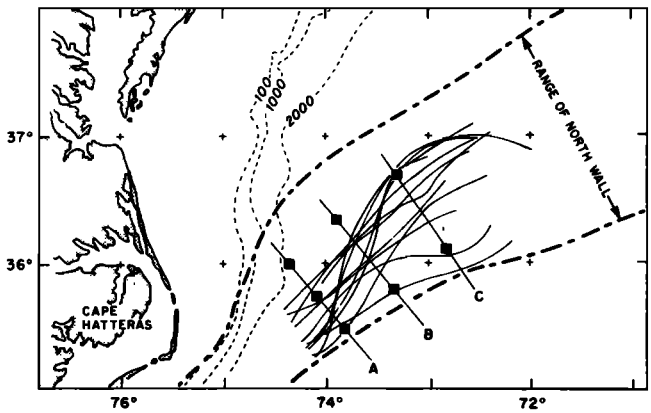


Fig. 1. Survey area. IES's are shown in black squares, along sections A, B, and C. Light solid lines are composite paths taken from 1979–1980 XBT surveys. The north wall envelope has been constructed from historical paths using shipboard (XBT and towed thermistor) and AXBT surveys.

repeated path segments at 26-hour intervals, using XBT data, in a 2° square near 70°W and delineated paths by airborne radiometer (ART) over much larger areas. They found fluctuations within a wide range of time scales. ART paths at intervals of a few days revealed a pattern of meanders migrating eastward at mean phase velocities of 5–8 cm $s^{-1}$, consistent with *Hansen*'s [1970] estimate. In addition, they observed one fluctuation with period ~6 days and wavelength ~250 km, indicating a rapid downstream propagation speed ~40 km $d^{-1}$. Periodicities as long as 80 days were estimated in association with large-scale secular shifts of the path.

*Halliwell and Mooers* [1979] used 2 years of weekly satellite infrared images, analyzed by the U.S. Naval Oceanographic Office ('Experimental Ocean Frontal Analysis' charts), to study the space-time structure and variability of the Gulf Stream surface temperature front from 74°W to 65°W. They find that the wave number spectrum is broadly peaked near wavelengths of 320 km, with which they associate propagation speeds of 6–7 km $d^{-1}$ and periods near 50 days.

To study variability with the observed range of time scales requires frequent sampling over a long period. In order to resolve the short-period fluctuations, the path should be determined at least every 2 days; however, logistical constraints make it impractical to maintain traditional surveys at this sampling interval for more than a few weeks. Moreover, to representatively sample the longer-period variations, a measurement program spanning at least 2 years is necessary.

## OBSERVATIONS

We have chosen to center our investigations just 100–200 km downstream of Cape Hatteras, where the meander envelope is known to expand rapidly, and yet where a moored array with a small number of instruments would coherently span and monitor variations within the stream. A study using moored instrumentation seemed necessary in order to meet the requirements discussed in the previous section. Satellite infrared imagery can produce extensive spatial coverage of the surface temperature contrasts. However, past studies have been limited by cloud cover, producing good images too infrequently to examine variability at periods shorter than ~14 days. Therefore they may suffer aliasing from higher-frequency fluctuations. Furthermore, our own direct observations have occasionally shown surface temperature patterns which have structures inconsistent with the position of the subsurface front at 200 m, which by convention indicates the path of the stream.

TABLE 1. Deployment Periods for Inverted Echo Sounders at the Sections Shown in Figure 1

| | IES's Number | | | |
|---|---|---|---|---|
| | May 1979 Deploy | August 1979 Recover | November 1979 Deploy | July 1980 Recover |
| Section A | 3 | 3 | 3 | 2 |
| Section B | 2 | 2 | 2 | 2 |
| Section C | 3 | 2 | 2 | 2 |

The instrument array which brings new capabilities to bear upon this Gulf Stream study consists principally of eight inverted echo sounders (IES). These instruments monitor the depth of the main thermocline acoustically from the seafloor, and when stationed under the sharply sloping thermocline associated with the Gulf Stream, they are able to track changes in its position (these techniques are discussed later). At least two IES's, spaced ~80 km apart, are required across the stream in this region to insure that at least one will always be under the strong cross-stream slope of the thermocline. Figure 1 indicates the instrument positions. The downstream spacing of the three sections was chosen conservatively to be 50 km because of our desire to obtain coherent records and on the basis that earlier observational records of the stream path did not show significant variability at shorter scales which would otherwise alias the measurements.

Our field operations and instrument deployment periods are summarized in Table 1, where the three sections have been identified on Figure 1. The IES array was first deployed for $3\frac{1}{2}$ months from May to August 1979, and seven of the eight instruments were recovered with good records. The center instrument along line C (not shown) failed and was not recovered. The second deployment was for 9 months (November 1979–July 1980) at the same seven sites, and six of those were recovered with good records. The center instrument along line A also failed. By good fortune the records along the northern and southern edges of the array were complete, so that the stream position was continuously tracked along each of the sections A, B, and C.

In addition to mooring work, a large volume of quasi-synoptic XBT data was collected during the cruises. Stream paths were delineated by criss-crossing the subsurface thermal front, or 'north wall' (indicated by 15°C at 200 m), at along-stream spacings of approximately 20 km, following the convention established by *Fuglister and Voorhis* [1965]. Detailed XBT sections were then taken normal to these paths. Altogether 12 path segments were mapped (shown in Figure 1), and 15 XBT sections were made. These data have been used below for calibration of the IES records and verification of the technique of monitoring the stream path within the array.

## METHODS

Inverted echo sounders were chosen, on the basis of earlier work [*Watts and Rossby*, 1977; *Watts and Olson*, 1978], to be deployed under the Gulf Stream. These instruments sit on the seafloor and transmit pulses of sound to

measure precisely the round trip acoustic travel time $\tau$ to the sea surface and back. The 10-kHz acoustic pulses are sent in a group of 32 pings each hour. Within this hourly burst sample, the median value of travel time is computed, with typically 0.3 ms uncertainty. Instrumental details are described more completely by *Bitterman and Watts* [1979]. Variations in $\tau$ (a few milliseconds) arise predominantly due to changes in the temperature and salinity profiles within the water column above the instrument. The travel time is an integral measurement $\tau = 2 \int_H^\eta C^{-1}\, dz$, where $H$ is bottom depth, $\eta$ surface height, and $C$ sound speed. Note that this is formally similar to the dynamic height integral, as discussed by *Watts and Rossby* [1977].

The travel time is affected principally by those internal displacements, which are vertically coherent throughout the water column, and is rather insensitive to features of small vertical scale. For example, the change in depth of the thermocline associated with a complete lateral shift of the Gulf Stream past an IES site causes a change in $\tau$ of 45 ms, whereas an extremely fresh cold feature 30 m thick with 10°C anomaly would only lengthen $\tau$ by 1 ms. Furthermore, those vertical displacements which have the greatest effect on $\tau$ are strongly weighted in the main thermocline, where $dT/dz$ is large; the conceptual discussion by *Watts and Rossby* [1977] formally emphasizes this fact. Because salinity affects the speed of sound in seawater relatively weakly, variations in travel time were shown to be proportional to variations in the thermocline depth, with a sensitivity of $-19.5$ m ms$^{-1}$ for the 12°C isotherm [*Rossby*, 1969]. *Watts and Wimbush* [1981] discuss the physical basis for this relationship. Additionally, if the surface height rises 1 m, $\tau$ lengthens by 1.3 ms. Such changes are caused primarily by surface tides and the baroclinic adjustment of the free surface across the stream, with perhaps a small effect arising from lower-frequency barotropic variability. For the purposes of this paper, the effects of surface (and internal) tides have been removed by low-pass filtering. We account for the baroclinic adjustment empirically, as described below.

Operationally, our procedure is to 'calibrate' the acoustic travel time measurements by taking XBT profiles over each of the IES sites in order to perform the regression $\xi = M\tau + B$, where $\xi$ is the depth of an isotherm within the main thermocline. For this study to conform with the traditional Gulf Stream path indicator we have chosen to work with the 15°C isotherm depth, which is slightly above the central part of the main thermocline. The $(\tau, \xi)$ correlation is not sensitive to which particular isotherm is chosen; both the 15°C and 12°C isotherm regressions yield a slope $M = -19.5$ m ms$^{-1}$. For any given IES site the intercept B in the regression depends upon the instrument depth and is determined by a least squares fit of the available XBT determinations of $Z_{15}$ $(=\xi)$ against the coincident values of $\tau$ recorded by the IES.

Figure 2 is a comparison of all direct $Z_{15}$ measurements obtained from XBT's and STD's within 1 mi of IES sites with the corresponding IES determinations of $Z_{15}$. The root mean square deviation is 20 m, which is small compared to the 800-m range over which $Z_{15}$ changes across the stream. Some of this departure is due to isotherm displacements on small lateral scales away from the IES site or on small vertical scales associated with higher-order internal modes. The vertical integration inherent to the $\tau$ measurements produces a $\xi$ (or $Z_{15}$) record which is rather insensitive to

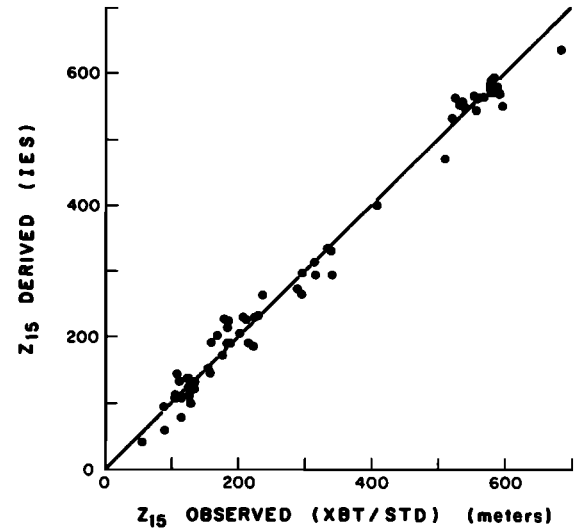


Fig. 2. IES derived 15°C depth versus observed 15°C depths. The rms deviation is ±20 m, taken from 61 points, in a range of 600 m.

such small vertical scale fluctuations, which may be advantageous.

With the set of $Z_{15}$ time series at each of the array sites, ones' first inclination in studying the variability might be to examine the coherence between sites. However, the amplitude of the $Z_{15}$ vertical displacement for a given meander is not directly proportional to the real (plan view) amplitude of that meander but depends upon the local cross-stream slope of the thermocline, i.e., the proximity of the north wall to the IES site. Therefore to examine properly meander propagation and growth, it is necessary to convert the cross-stream pairs of $Z_{15}$ series on the three sections A, B, C into time series of lateral displacements of the stream path. For these purposes we used the mean section of the Gulf Stream shown in Figure 3, which was produced from 15 XBT sections made in our study region, each of which was normal to the instantaneous path immediately preceding the section. To obtain a mean section representative of the instantaneous

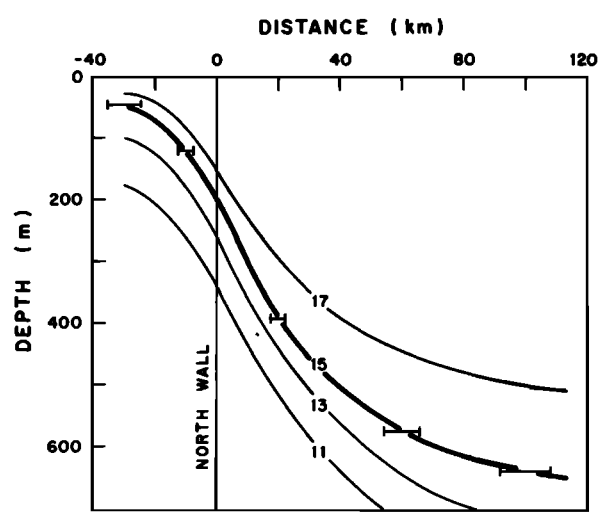


Fig. 3. Mean profile of the upper main thermocline constructed from 15 sections normal to the instantaneous path of the Gulf Stream. Distances are measured relative to the 'north wall' (15°C/200 m). The error bars shown at various points along the 15°C curve represent one standard deviation.

cross section rather than a broadened geographic average, the individual sections were shifted to align their 'north wall' positions. The heavy line in Figure 3 emphasizes the functional form of the mean 15°C profile across the stream. Knowing $Z_{15}$ at any one IES site, we thus produce an estimate of the position of the north wall relative to that site. Using two or three sites across the stream, we make a better estimate along the section joining them as a weighted average from all sites, with weights proportional to the inverse square error bars of the mean 15°C profile. In this manner, time series of the north wall position $X(t)$ along each line A, B, C are calculated, increasing positively relative to the origin at the northern IES on each line. An example of the conversion from $Z_{15}$ series to $X(t)$ for section A, May to August 1979, is shown in the appendix. Also shown in the appendix are the very consistent displacement realizations obtained when either two or three of the IES's making up section A are used in the weighted average calculation.

How well does this procedure work, and to what extent might the $X(t)$ series contain artifacts due to anomalous lenses of water advecting through the array? Relatively large changes in $\tau$ (15 ms) occur in the records on time scales of 3–5 days. Such changes can only be due to lateral translations of the stream, as they would otherwise require inordinately large anomalies: For example, an increase of even 5 ms would require an anomalous lens of cold water with 5°C anomaly 300 m thick, which is inconsistent with any existing hydrographic work in this region of the stream.

Most importantly, we have several direct comparisons between the positions of the north wall surveyed by zig-zag ship tracks and those estimated along lines A, B, and C by the IES array. The rms difference between ship and IES determinations of position is 8 km. This uncertainty is consistent with an error estimate from the combined uncertainty in the $Z_{15}$ (20 m) and in the mean 15° profile (see Figure 3 error bars), and the weighted averaging procedure, as explained in the appendix.

We believe, in fact, that the actual (dynamically important) noise level in the path determinations is approximately 5 km because of the high coherences between $X(t)$ records at successive downstream sites. For example, the statistical upper bound on the rms measurement noise, $\sigma_{max}$, is $\sigma_{max} = S(1 - \gamma)/\gamma$, where $S$ is the rms displacement signal and $\gamma$ is the coherence [*Bendat and Piersol*, 1971]. Using the observed coherence $\gamma \gtrsim 0.8$ (shown later) for the displacements on IES sections B and C at the energetic periods of 4 days and longer, where the rms lateral displacement is 20 km, yields $\sigma_{max} \sim 5$ km. Thus while ship surveys of $Z_{15}$ may fluctuate by 8 km, the vertically integrated view of the front, as provided by the IES's, is more characteristic of the dynamically significant stream path throughout the length of the array than would be the measurement of the depth of any single isotherm. This advantage is similar to that of dynamic height integrals.

## RESULTS

Figure 4 shows the time series $X(t)$ at sections A, B, and C, indicating where the north wall crosses each section as a function of time, for May–August 1979 and November 1979–July 1980. The zero displacement on each line is taken to be at the northwestern IES site along the line, as identified on Figure 1. A positive $X$ is a displacement offshore toward the Sargasso Sea. The records have been low-pass filtered by convolution with a 24-hour Gaussian weighted window.

The stream's fluctuations have a variety of periodicities, which are evident in Figure 4. Several events clearly travel downstream, as indicated by the lag between their occurrences in the records (for example, near May 20, August 3, November 16, January 25, and several other cases) when examined carefully. The translation speed for these primarily short-period ($\lesssim$10 day) features is typically 35 km $d^{-1}$; coherence calculations discussed later develop this subject further.

To better illustrate the variety of stream paths represented by the time series in Figure 4, a sequence of plan views of the path is presented in Figure 5. In each frame the stream positions $X(t)$ along each section A, B, and C have been connected by a smooth curve, and for visual reference, six IES sites and a rhumb line, which indicates the historical mean north wall path, are repeated. The frame interval, 23

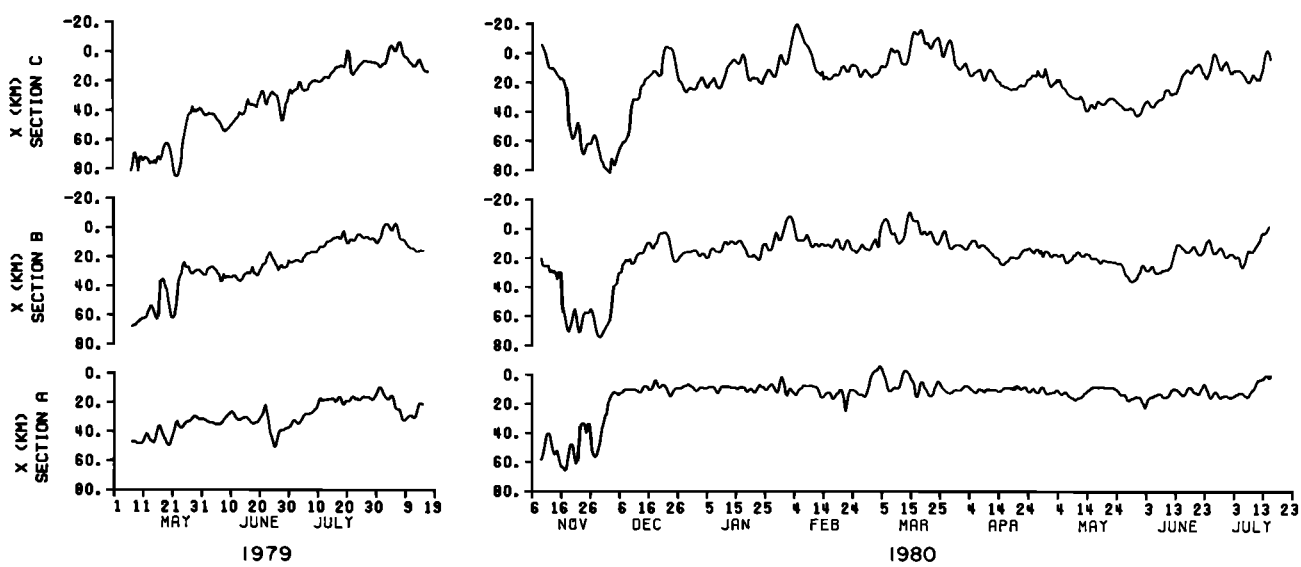


Fig. 4. Time series of displacements $X$ at sections A, B, and C. All series have been low passed with a 24-hour bandwidth Gaussian filter.

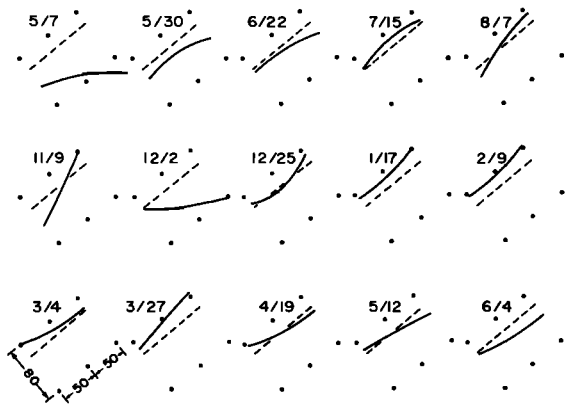


Fig. 5. Sequence of plan view Gulf Stream paths at 23-day intervals, relative to IES sites (shown as solid circles) and rhumb line (dashed) indicating the mean location of the north wall. The corresponding dates are labeled in the upper left-hand corner of each frame. Paths are drawn as smooth curves through the north wall positions along each of the sections.

days, is insufficient to follow the development of meanders but is chosen to illustrate that the stream can flow nearly north (11/9) or east (12/2) through the array with significant cyclonic or anticyclonic curvature as large as $0.98 \times 10^{-2}$ km$^{-1}$ (12/25) or respectively $-0.91 \times 10^{-2}$ km$^{-1}$ (7/15). The corresponding path curvature vorticity associated with near-surface waters moving 2 m s$^{-1}$ would be ~25% of the planetary vorticity in magnitude.

The long-period (~50 day) meander of Figure 4 in November–December 1979 is displayed in Figure 6 as a sequence of paths at 2-day intervals. Even at this 2-day sampling rate, some small-scale features move rapidly through the array and alias the representation slightly. However, one can see the dominant passage of a trough, followed by a crest, and the start of another trough through the array. This longer-period feature translates downstream at about 15–20 km d$^{-1}$, which is considerably slower than the propagation of short-

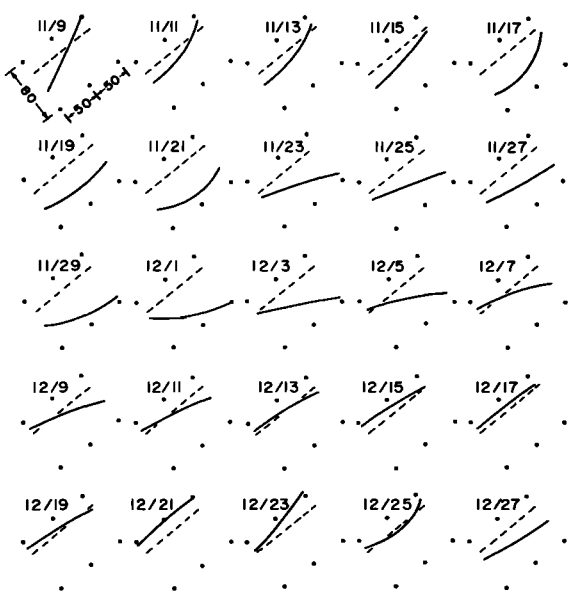


Fig. 6. Sequence of plan view paths as in Figure 5, but at 2-day intervals, showing the passage of a large perturbation through the array in November–December 1979.

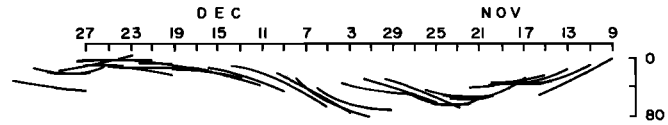


Fig. 7. Alternate view of the same sequence of paths shown in Figure 6. Each path segment is drawn relative to a constant rhumb line through the IES array but offset 30 km upstream every 2 days to illustrate the basic waveform of this large meander.

period (4–10 day) fluctuations. Figures 4 and 6 also illustrate how rapidly the stream can shift laterally. Lateral velocities of ~20 km d$^{-1}$ were observed on several occasions, e.g., May 25, 1979, and December 15, 1980 (Figure 4). This has made it difficult in the past to obtain truly synoptic data.

The wavelike nature is emphasized by another presentation of these data in Figure 7, which aligns the dashed lines of each frame from Figure 6 and offsets each instantaneous path in time to the left. The distance offset (30 km) and time interval (2 days) correspond to a downstream translation of 15 km d$^{-1}$. Superimposed on this basic wave are small-scale perturbations, which tend to translate more rapidly (see November 19–23 or December 23–27). By contrast, the large perturbation intensified in place briefly on November 27–29. Satellite imagery indicates that this large perturbation apears to have been forced by interaction with a warm core Gulf Stream ring. *Cornillon* [1982] reports good agreement between tracking of the stream by satellite and IES during this period.

The path displacement records of Figure 4 have the corresponding power spectral densities shown in Figure 8. In order to combine results from the two deployment periods,

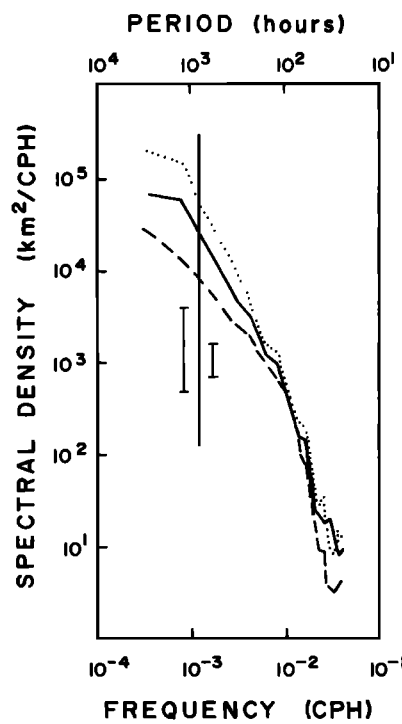


Fig. 8. Ensemble-averaged power spectra of path displacements at sections A (dashed), B (solid), and C (dotted), incorporating 32 degrees of freedom for $T \leq 800$ hours and 8 degrees of freedom for $T > 800$ hours. The error bar indicates the 90% confidence interval.

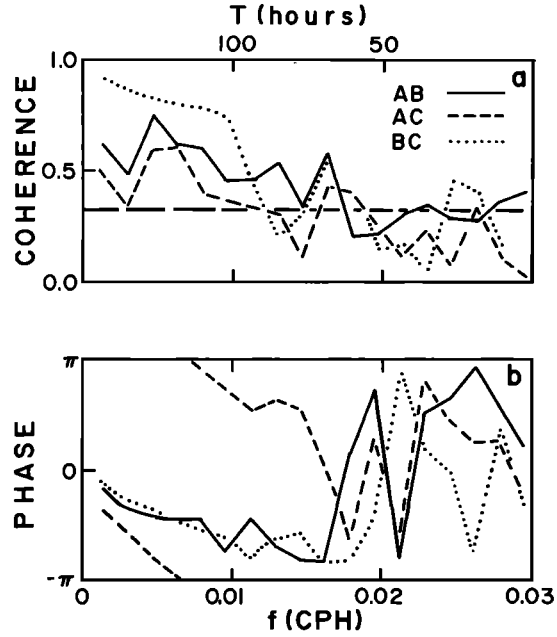


Fig. 9. Ensemble averaged coherence (Figure 9*a*) and phase (Figure 9*b*) between pairs AB (solid), AC (dashed), and BC (dotted). Heavy dashed line at 0.32 in Figure 9*a* indicates the 90% significance level for a random process.

these spectra are ensemble averages from four 3-month members at the sections A, B, C. Each member was detrended and windowed with a cosine taper function on the first and last 10% of the record prior to computing the Fourier transform, in order to suppress nonstationary effects and leakage. Four adjacent bands were averaged within each member, so that the ensemble spectra have approximately 32 degrees of freedom. At periods shorter than 100 hours the spectra at all three sections are very similar and fall off very rapidly with a slope of about −4. At periods longer than 100 hours the slope is −1 to −2. Over 96% of the variance is associated with periods longer than 4 days, and the variance doubles with each 50-km step downstream. Root mean square displacements were 15, 20, and 30 km, respectively, progressing downstream. During each time period from which the ensemble meanders were drawn (May–August, November–January, February–April, May–July), the same pattern of downstream growth obtained (not shown), without significant structure in the spectra other than the dominance of long periodicities. The 90% confidence limits show the downstream growth to be significant, and a runs test on the variance confirms that these spectral shapes and the spatial growth are not biased by nonstationary bursts of variance.

Coherence and phase delays between each pair of sections are shown in Figure 9. These were calculated as cross-spectral averages from the same four 3-month ensemble members described above. The results were found to be statistically the same for each ensemble member, indicating that they are drawn from the same statistical process and not biased by any one member. In all cases the coherences are significant (>0.32) at the 90% confidence level for periods longer than 4 days. The pairs AB and BC, separated by 50 km, have the greatest coherences and very similar phase relationships. The downstream pair BC is even more coherent than the upstream pair AB because the meander signal has grown to overwhelm the 'noise' within the extra 50 km distance downstream. ('Noise' here is considered to be both measurement error and any nonpropagating fluctuations.) The pair AC separated by 100 km is slightly less coherent (but still significant to $T = 4$ days), and the phase delays shown in Figure 9 are double those of the pairs 50 km apart.

The sense of the phase lag $\phi$ is such that the meanders are translating downstream. The phase speed may be determined as $c_r = \delta x \cdot (2\pi f/\phi)$, where $\delta x$ is the downstream spacing between lines. Close examination of Figure 9 at the highly coherent low frequencies reveals, from the positive curvature of the phase lines, that $\phi/f$ becomes larger in magnitude at low frequencies. These changes are not statistically distinct at the 90% confidence level, but in all three cases the tendency is for long-period fluctuations to propagate more slowly, e.g., $c \sim 20$ km d$^{-1}$ at $T = 800$ hours and $c \sim 40$ km d$^{-1}$ at $T = 100$ hours.

It is instructive to represent the above results in terms of propagating waves $\propto \exp(i(k_n y - \omega_n t))$, with downstream growth represented by a complex wave number $k_n = k_{rn} - i\kappa_n$, $\kappa_n > 0$. If any constituent $n$ is viewed in a frame of reference moving at speed $c_{rn} = \omega_n/k_{rn}$ with $y' = y + c_{rn}t$, then $i(k_n y - \omega_n t) = ik_{rn}y' + \sigma_n t$, where $\sigma_n = \kappa_n c_{rn}$ is the temporal growth rate in that moving frame. The frequency spectra (with spatial growth) which we have measured in a fixed array may thus be viewed, using the observed phase lags or propagation speeds, in terms of wave numbers associated with those frequencies. In the moving frame there

TABLE 2. Dispersion Relationship and Growth Rates for Gulf Stream Meanders Estimated From the Phase Delays and Spectral Densities at Three Cross-Stream Sections

| $f$, cpd | $T$, days | $c_r$, km d$^{-1}$ | $k_r$, 10$^{-2}$ km$^{-1}$ | λ, km | $\kappa$, 10$^{-3}$ km$^{-1}$ | $\sigma$, d$^{-1}$ | $c_i$, km d$^{-1}$ | $c_g$, km d$^{-1}$ |
|---|---|---|---|---|---|---|---|---|
| 0.03 | 33.3 | 20 | 0.96 | 653 | 8.2 | 0.16 | 17 | ... |
| | | 28 | 0.68 | 920 | 7.9 | 0.22 | 32 | ... |
| 0.07 | 14.3 | 28 | 1.58 | 398 | 6.1 | 0.17 | 11 | 44 |
| | | 28 | 1.56 | 403 | 6.1 | 0.17 | 11 | 36 |
| 0.11 | 9.1 | 32 | 2.16 | 291 | 3.2 | 0.10 | 5 | 47 |
| | | 34 | 2.01 | 312 | 1.2 | 0.04 | 2 | 51 |
| 0.15 | 6.7 | 35 | 2.66 | 236 | 1.8 | 0.06 | 2 | 59 |
| | | 37 | 2.58 | 243 | 1.7 | 0.06 | 2 | 52 |
| 0.19 | 5.3 | 40 | 3.01 | 208 | 2.6 | 0.10 | 3 | 58 |
| | | 40 | 2.98 | 211 | 1.6 | 0.06 | 2 | 61 |
| 0.23 | 4.3 | 41 | 3.55 | 177 | 2.9 | 0.12 | 3 | ... |
| | | 42 | 3.42 | 184 | 3.9 | 0.16 | 5 | ... |

For each frequency and period the first line is from sections A and C separated by 100 km downstream; the second line is from sections B and C separated by 50 km downstream.

is temporal growth, with a corresponding complex wave speed, $c = c_r + ic_i$ with $c_{in} = (\kappa_n/k_{rn})c_{rn}$.

All the above terms may be estimated from the spectra and cross spectra at the three sections A, B, and C. The phase speed may be obtained from the phase lag: $c_n = \omega_n \delta x/\phi_n$. The spatial growth rate may be estimated from the ratio of the smoothed spectral estimates $G_2/G_1 = \exp 2\kappa(x_2 - x_1)$, so $\kappa = \ln (G_2/G_1)/2\delta x$. Table 2 summarizes these results, with the subscript $n$ dropped.

The phase speeds of 20–40 km $d^{-1}$ are intermediate between slower propagation speeds which have been reported farther downstream, ~5 to 10 km $d^{-1}$ [*Hansen*, 1970; *Robinson et al.*, 1974], and faster speeds upstream, ~35–40 km $d^{-1}$ [*Brooks and Bane*, 1981]. Growth rates observed by Hansen farther downstream were smaller, $\kappa \sim (2 \pm 1) \times 10^{-3}$ $km^{-1}$ (for $\lambda \simeq 300$ km), and rates predicted theoretically by *Tareev* [1965] and *Orlanski* [1969] were $\kappa = 8 \times 10^{-3}$ $km^{-1}$ ($\lambda = 250$ km) and $\kappa = 12 \times 10^{-3}$ $km^{-1}$ ($\lambda = 365$ km), respectively. A time-dependent thin jet model by *Robinson et al.* [1975] found for (31 day, 560 km) perturbations the corresponding downstream $e$-folding scale was $\kappa = 5 \times 10^{-3}$ $km^{-1}$ in good agreement with these observations.

Figure 10 plots the real and imaginary phase speeds ($c_r$, $c_i$) and the spatial and temporal growth rates ($\kappa$, $\sigma$) as a function of downstream wave number $k_r$, all estimated from our data as described above. The uncertainty in $c_r$ and $k_r$ is typically ±25% except for the lowest frequency estimate, which is ±75%. The uncertainty in $\kappa$ is about ±30%, in $\sigma$ ±50%, and in $c_i$ nearly 100%. The shape of the $c_r(k)$ curve is remarkably similar to *Phillips*' [1954] two-layer quasi-geostrophic model of baroclinic instability. Physically, only disturbances with wavelengths much longer than the Rossby internal deformation scale, $\lambda_{Ro}$, can extract baroclinic energy from the flow, but as wavelengths increase, the $\beta$ effect slows and eventually stabilizes the waves [*Pedlosky*, 1979]. We identify growth at wavelengths as short as 180 km and as long as 600 km. The amplitudes exhibit temporal $e$-folding in 6–10 days, which is comparable to *Hansen*'s [1970] earlier estimate of $\sigma = 2 \times 10^{-6}$ $s^{-1}$. The group speed (also shown in Figure 10) may be estimated by finite difference, from $c_g = c_r + k_r \partial c_r/\partial k_r$, to increase from 45 km $d^{-1}$ at $\lambda = 350$ km to 60 km $d^{-1}$ at $\lambda =$ 200 km. The uncertainty in $c_g$ is ±35%. Our observed phase and group speeds are similar to those theoretically predicted by *Tareev* [1965] but a factor of 2 to 4 larger than by *Orlanski* [1969].

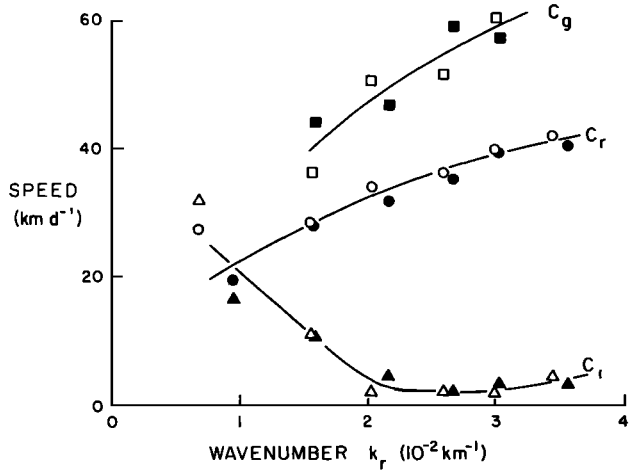


Fig. 10*a*. Phase speed components ($c_r$, $c_i$) and group speed ($c_g$) plotted versus wave number $k_r$. Open circles, triangles, and squares represent $c_r$, $c_i$, and $c_g$, respectively, calculated at 50-km separation between sections B and C. Solid circles, triangles, and squares represent $c_r$, $c_i$, and $c_g$ at 100-km spacing between sections A and C.

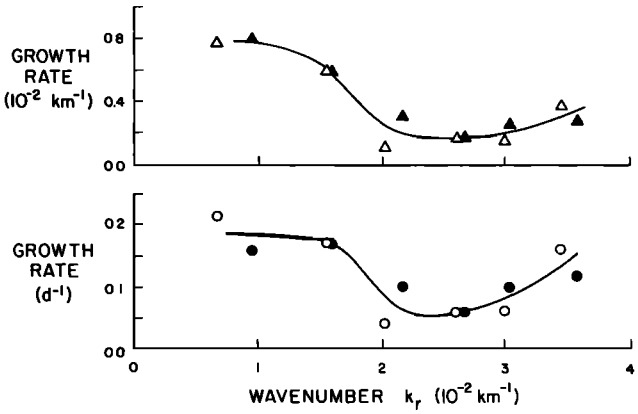


Fig. 10*b*. Spatial growth rate $\kappa$ (triangles) and temporal growth rate $\sigma$ (circles), plotted versus wave number $k_r$. Open and solid symbols are for sections BC and AC, respectively, as in Figure 10*a*.

The dispersion relationship indicated by Table 2 and Figure 10 is statistically the best fit describing propagating, growing waves. The observed high coherence of the path displacements $X_i(t)$ suggests that the downstream path $x$ ($y$, $t$) should be predictable from knowledge of the dispersion relation applied to 'inlet' observations such as ours. Work is in progress to test this; however, one should note by careful examination of the $X_i(t)$ time series in Figure 4 that some of the perturbations do not grow as they move downstream. Moreover, fluctuations could develop downstream of the 'inlet' and decrease the downstream coherence and predictive accuracy.

The spatial growth rate $\kappa$, listed in Table 2, indicates that for periods and wavelengths ($T$, $\lambda$) shorter than (9 days, 300 km), the fluctuations $e$-fold in a distance long compared to the wavelength. However for ($T$, $\lambda$) longer than (14 days, 400 km) the $e$-folding growth occurs in less than a wavelength, and consequently, the growth may be more appropriately described as temporal. The temporal growth rate $\sigma^{-1}$ ranges from 6 to 14 days, weakly dependent upon period or wavelength (Table 2).

The fastest growth is associated with ($T$, $\lambda$) greater than (9 days, 300 km) and in a band near (4 days, 180 km). This description and Figure 10 closely resemble the theoretical results for baroclinically unstable disturbances shown by *Hogg* [1976], in which he indicates a transition at $k = 2.4 \times 10^{-2}$ $km^{-1}$ from spatial growth for shorter ($T$, $\lambda$) to temporal growth for longer ($T$, $\lambda$). The wave number at which this transition occurs corresponds closely to the high wave number growth cutoff in Phillips' model, for an appropriate choice of length scale, ~ $2\lambda_{Ro}$. *Pedlosky* [1979] treats several other baroclinic instability models, in all of which the fluctuations propagate as exp $ik(x-ct)$ with $k$ real and $c$ complex, and in which the temporal growth $\propto$ exp $kc_i t$ exhibits a high wave number cutoff $k_T$. By contrast, as shown by Hogg, instabilities which include complex $k$ can exhibit spatial growth at wave numbers greater than the temporal growth cutoff ($k \geq k_T$). Although our measurements do not indicate a clear distinction between temporal and spatial growth, the observed local minimum in growth

rate near $k = 2.4 \times 10^{-2}$ km$^{-1}$ closely resembles the transition from temporal to spatial growth predicted by Hogg. The great similarity between our observations and the foregoing theories suggests that the baroclinic instability mechanism is operative in the Gulf Stream and that realistic models should include spatial as well as temporal growth.

## CONCLUSIONS

An array of IES's moored beneath the Gulf Stream has proven to be successful in continuously determining the stream path and monitoring its spatial and temporal variability. The measurements are unique in that they provide continuous tracking of the upper layer thermal front for a year in conjunction with current and temperature records in the deep waters. This combined data set allows us to study the relationship of the deep currents to near-surface path displacements; this is discussed in a subsequent paper (W. E. Johns and D. R. Watts, manuscript in preparation, 1982). Our emphasis in this paper has been on the IES data, from which we have been able to estimate the dispersion relation for Gulf Stream meanders in our observational area off Cape Hatteras, North Carolina (Figure 10).

During the IES deployments, we made careful comparisons with traditional shipboard methods of tracking the stream, as discussed in the methods section, and feel that the validity of the technique has been proven. The IES array was set to determine the lateral displacement records $X(t)$ along three cross-stream sections at alongstream spacings of 50 and 100 km. This conservative spacing was small enough to produce highly coherent records, yet was great enough to measure the downstream phase lags with sufficient accuracy to estimate translation speeds. The energy-containing meanders have periods $\gtrsim$4 days and wavelengths $\gtrsim$150 km; hence our results are neither temporally nor spatially aliased by smaller scales.

This set of measurements has thus provided a statistical (ensemble average), rather than deterministic, description of meanders as waves propagating downstream with the following characteristics. Path displacements exist on a continuum of time scales between 2 and 60 days with over 96% of the variance at periods longer than 4 days. Lateral velocities of the stream axis are largest in the band 4–10 days and decrease gradually at longer periods. Propagation is downstream in all cases, varying between 40 km d$^{-1}$ at short periods and wavelengths (4 days, 180 km) to 20 km d$^{-1}$ associated with (30 days, 600 km) meanders. These speeds are intermediate between values measured upstream along the Carolina Shelf (35–40 km d$^{-1}$) and those estimated farther downstream (5–10 km d$^{-1}$). Propagation rates of less than 30 km d$^{-1}$ are apparently found only in association with growing meanders in deep waters northeast of Cape Hatteras.

Rapid downstream growth was observed, doubling the total variance in each 50-km interval downstream. The growth was entirely associated with periods longer than 4 days and greatest for periodicities of 14 days and longer. The minimum growth rate observed near $k = 2.4 \times 10^{-2}$ km$^{-1}$ is very similar to the behavior predicted by *Hogg* [1976]. His theory has a high wave number cutoff for temporally growing baroclinic instabilities, in agreement with similar preceding theories, but additionally includes spatial growth at higher wave numbers.

In summary, this work has provided the first observational dispersion relation for Gulf Stream meanders, against which theoretical and numerical results may be tested.

## APPENDIX: DETERMINATION OF THE GULF STREAM POSITION

Lateral displacements of the stream axis are calculated as a weighted average $\bar{X} = \Sigma_N W_i X_i / \Sigma_N W_i$ of the displacement estimates $X_i$ from each of the $N(= 2$ or 3) IES's across the stream. The $W_i$ are smoothed weights proportional to the local inverse variance of the mean profile (Figure 3). Thus for each $Z_{15}$ measured by an IES there are corresponding $X_i$ and $W_i$ as specified by the mean 15°C profile. In the $Z_{15}$ range 150–400 m the thermocline slope is larger by a factor of 2 or more than that in outer regions of the profile, and the error bars (representing one standard deviation from the mean of 15 sections observed in this region) are less than 2.0 km. An IES located under this 30-km-wide portion of the Gulf Stream will provide $X_i$ estimates consistently accurate to $\leq$5 km and will, by design, heavily outweigh neighboring instruments in the $\bar{X}$ calculation. Somewhat less accurate determinations ($\pm$10 km) can be expected when only two IES's, separated by 80 km, are used and the stream is positioned such that they each lie under the 'tails' of the profile. Knowledge of the mean path and the range of lateral excursion of the Gulf Stream in a selected region helps to

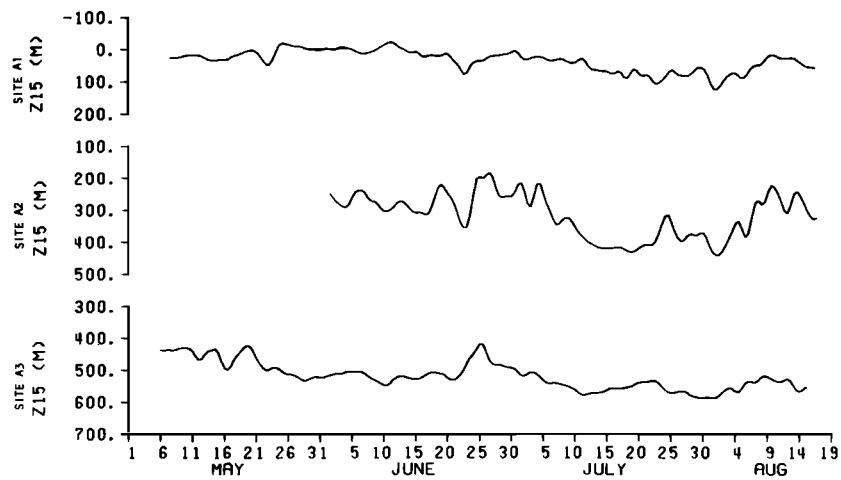


Fig. 11. $Z_{15}$ records at IES sites $A_1$, $A_2$, and $A_3$; May–August 1979.

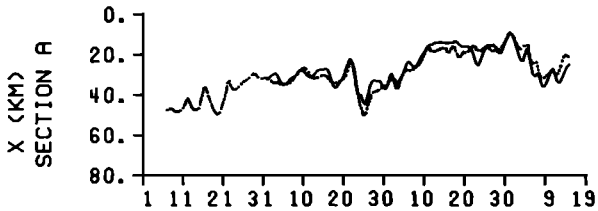


Fig. 12. Comparison of weighted average displacement records along line A, using all three IES's (solid) or only the two endpoint IES's A1 and A3 (dotted).

determine the optimum placement of instruments, so that these errors may be minimized.

The method is illustrated for the time period May–August 1979, when three IES's were located along section A. The $Z_{15}$ time series at IES sites A1, A2, and A3 (proceeding from northwest to southeast along section A, respectively), are shown in Figure 11. A2 (deployed approximately 1 month later than the others) clearly has the largest dynamic range because it is usually near the stream center and appears to contain fluctuations not present in either A1 or A3. Its $Z_{15}$ values lie in the steep 200–400 m range. Conversely, A1 rarely exceeds 100 m and A3 is everywhere deeper than 400 m. Calculations of $\bar{X}$ using (1) only A1 and A3 or (2) A1, A2, and A3 are shown in Figure 12. They are remarkably similar considering the overriding weight of A2 in the latter series. The largest differences are 0(5 km), and, most importantly, all the major fluctuations are reproduced in both series.

Passage of the stream axis at an oblique angle through IES sections is also handled well computationally by the weighted average technique. For example, angles as large as 30° relative to normal were occasionally observed. From each IES we obtain an estimate of the distance $R_i$ to the stream axis along a line normal to the instantaneous path. It follows from simple geometric considerations (Figure 13) that for a given stream angle $\theta$, each IES underestimates the true along-section distance to the stream axis by an amount $\Delta_i = X_i (1 - \cos \theta)$, i.e., each by the same fraction of their respective $X_i$. The average $\bar{X}$ is therefore close to the true position $X$. This works particularly well when the stream is located so that both weights $W_i$ are relatively significant. Otherwise, one IES will be very close to the axis, consequently dominating the average, and the error (proportional to that $X_i$) will again be small. We conclude that only when the stream axis strays more than approximately 20 km outside the bounds of the array will errors arising from nonnormal intersection angles be comparable with those introduced by variability in the cross-stream structure. Maximum estimated stream curvatures were 1/110 km$^{-1}$; their effect is negligible in the position-error analysis.

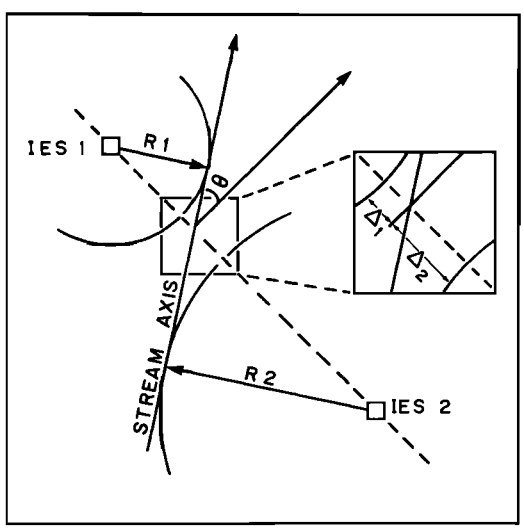


Fig. 13. Geometrical representation of the Gulf Stream axis passing through IES section, with ranges from the instantaneous path denoted by R1 and R2. When the stream is not normal to the section, but passes at oblique angle $\theta$, each IES underestimates its proximity to the axis by $\Delta$ (see inset). The weighted average is between the two estimates and is a close approximation to the true axis position.

A cross-stream section of two IES's spaced 80 km apart therefore provides an effective lateral tracking range of 120 km over which probable errors are 0(5 km). This estimate is supported by direct intercomparisons as discussed in the methods section.

*Acknowledgments.* This work has been supported by the National Science Foundation under grants OCE 78-09655 and OCE 79-21029. We would like to thank Elizabeth Johns and Jorge Vasquez, graduate students at the University of Rhode Island, for their help, and acknowledge the able assistance of the captain and crew aboard R/V *Endeavor* on several cruises helping to assure our success. The inverted echo sounders were carefully prepared by Michael Mulroney.

## REFERENCES

Bane, J. M., Jr. and D. A. Brooks, Gulf Stream meanders along the continental margin from the Florida Straits to Cape Hatteras, *Geophys. Res. Lett.*, *6*(4), 280–282, 1979.

Bane, J. M., Jr., D. A. Brooks, and K. R. Lorenson, Synoptic observations of the three-dimensional structure, propagation, and evolution of Gulf Stream meanders along the Carolina continental margin, *J. Geophys. Res.*, *86*, 6411–6425, 1981.

Bendat, J. S., and A. G. Piersol, *Random Data: Analysis and Measurement Procedures*, pp. 142–143, Interscience, New York, 1971.

Bitterman, D. S., and D. R. Watts, The inverted echo sounder, *IEEE Oceans '79*, 302–306, Sept. 1979.

Brooks, D. A., and J. M. Bane, Jr., Gulf Stream fluctuations and meanders over the Onslow Bay upper continental slope, *J. Phys. Oceanogr.*, *11*(2), 247–255, 1981.

Cornillon, P., The edge of the Gulf Stream: Satellite versus inverted echo sounder determinations, *Eos Trans. AGU*, *63*, 363, 1982.

Fuglister, F. C., Gulf Stream '60, *Prog. Oceanogr.*, *1*, 265–373, 1963.

Fuglister, F. C., and A. D. Voorhis, A new method of tracking the Gulf Stream, *Limnol. Oceanogr.*, *10*, R115–R124, 1965.

Fuglister, F. C., and L. V. Worthington, Some results of a multiple ship survey of the Gulf Stream, *Tellus*, *3*, 1–14, 1951.

Halliwell, G. R., Jr., and C. N. K. Mooers, The space-time structure of the shelf water-slope water and Gulf Stream surface temperature fronts and associated warm-core eddies, *J. Geophys. Res.*, *84*, 7707–7725, 1979.

Hansen, D. V., Gulf Stream meanders between Cape Hatteras and the Grand Banks, *Deep Sea Res.*, *17*, 495–511, 1970.

Hogg, N. G., On spatially growing baroclinic waves in the ocean, *J. Fluid Mech.*, *78*, 217–235, 1976.

Legeckis, R. V., Satellite observations of the influence of bottom topography on the seaward deflection of the Gulf Stream off Charleston, S.C., *J. Phys. Oceanogr.*, *9*, 483–497, 1979.

Orlanski, I., The influence of bottom topography on the stability of jets in a baroclinic fluid, *J. Atmos. Sci.*, *26*(6), 1216–1232, 1969.

Pedlosky, J., *Geophysical Fluid Dynamics*, 624 pp., Springer-Verlag, New York, 1979.

Phillips, N. A., Energy transformations and meridional circulations associated with simple baroclinic waves in a two-level quasi-geostrophic model, *Tellus*, *6*, 273–286, 1954.

Robinson, A. R., J. R. Luyten, and F. C. Fuglister, Transient Gulf Stream meandering, I, An observational experiment, *J. Phys. Oceanogr., 4,* 237–255, 1974.

Robinson, A. R., J. R. Luyten, and G. Flierl, On the theory of thin rotating jets: A quasi-geostrophic time-dependent model, *Geophys. Fluid Dyn., 6,* 211–244, 1975.

Rossby, H. T., On monitoring depth variations of the main thermocline acoustically, *J. Geophys. Res., 74,* 5542–5546, 1969.

Tareev, B. A., Unstable Rossby waves and the instability of oceanic currents, *Izv. Acad. Sci. USSR Atmos. Oceanic Phys. Engl. Transl., 1*(4), 426–438, 1965.

Watts, D. R., and D. B. Olson, Gulf Stream ring coalescence with the Gulf Stream off Cape Hatteras, *Science, 202,* 971–972, 1978.

Watts, D. R., and H. T. Rossby, Measuring dynamic heights with inverted echo sounders: results from MODE, *J. Phys. Oceanogr., 7*(3), 345–358, 1977.

Watts, D. R., and M. Wimbush, Sea surface height and thermocline depth variations measured from the sea floor, paper presented at the International Symposium on Acoustic Remote Sensing of the Atmosphere and Oceans, Univ. of Calgary, Calgary, Alberta, June 22–25, 1981.

(Received August 25, 1981;
revised August 23, 1982;
accepted August 23, 1982.)